JOURNAL OF MATERIALS SCIENCE 32 (1997) 1169–1175

Influence of the nature of microconstituents on the tensile properties of a zinc-based alloy and a leaded-tin bronze at different strain rates and temperatures

B. K. PRASAD, A. H. YEGNESWARAN
Regional Research Laboratory ''(CSIR)'' Habibganj Naka, Bhopal 462 026, India
A. K. PATWARDHAN
Metallurgical Engineering Department, University of Rookee, Roorkee 247 667, India

An attempt has been made to study the influence of the nature of microconstituents, strain rate and test temperature on the tensile properties of a zinc-based alloy (ZA 27). The properties of the alloy have been compared with those of a (leaded-tin) bronze (SAE 660) under similar test conditions. In the latter case, one of the phases (lead) has rather poor compatibility with the matrix. Properties such as hardness, density and electrical conductivity of the alloys have also been measured. The microstructure of the zinc-based alloy revealed primary α-dendrites surrounded by the eutectoid $\alpha + \eta$ in the interdendritic regions. The metastable ε phase was also present. The bronze revealed primary α-dendrites together with the Cu–Sn intermetallic in the interdendritic regions. Discrete particles of lead were also observed in the microstructure of the bronze. Increasing test temperature caused a reduction in the ultimate tensile strength (UTS) and an increase in the ductility of the alloys, the zinc-based alloy being much more influenced than the bronze. Higher strain rates revealed improved strength and percentage elongation in which the zinc-based alloy was once again influenced more than the bronze. A comparison of the tensile properties revealed the UTS of the zinc-based alloy to be higher than that of the bronze at lower test temperatures while the trend reversed at higher temperatures. However, the percentage elongation of the former was always higher. Tensile fractured surfaces revealed the occurrence of material failure by a mixed mode, i.e. ductile and brittle type. The bronze specimens exhibited microcracking along the lead/matrix interfacial regions at low test temperatures. Fracture of lead was also observed in this case. However, this tendency was somewhat suppressed at higher test temperatures. The contribution of ductile fracture in the case of the zinc-based alloy was more than the bronze in general, whose extent increased at higher test temperatures. Coarsening of the dimples was another observation made at elevated test temperatures in the case of the zinc-based alloy. The behaviour of the alloys has been explained in terms of their microstructural and fractographic features. An attempt has also been made to understand the mechanisms of material failure.

1. Introduction

Zinc-based alloys comprising 8%–28% aluminium together with 1%–3% copper, have been found to be a cost- and energy-effective substitute for conventional (leaded-tin) bronzes in a variety of engineering applications [1–5]. They have been popular owing to a number of advantages such as light weight, lower cost and better performance when compared with their conventional bronze counterparts under specific service conditions [1–5].

Physical and mechanical properties of zinc-based alloys have been compared with those of (leaded-tin) bronzes at room temperature in many investigations (1, 3, 5–9), while limited information is also available pertaining to the influence of test temperature on the tensile properties of zinc-based alloys [6, 10–16]. However, attempts made towards understanding the mechanisms of material failure in the alloys are still very limited [10, 11, 16–20].

In view of the above observations, an attempt has been made to examine the response of a zinc-based alloy and a leaded-tin bronze at different strain rates and test temperatures. Properties such as density, hardness and electrical conductivity of the alloys were also measured.

The behaviour of the alloys has been explained on the basis of their microstructural and fractographic features.

0022–2461

2. Experimental procedure

2.1. Alloy preparation

Alloys (Table I) were prepared by a liquid metallurgy route in the form of (20 mm diameter, 150 mm long) cylindrical castings using permanent moulds. Special high-grade (99.99% pure) zinc was used for alloy preparation. Other elements used were 99.95% pure.

2.2. Microscopy

Small (20 mm diameter, 15 mm long) specimens were cut from the castings and polished according to standard metallographic techniques. This was followed by etching the specimens. The specimens of the zinc-based alloy were etched with diluted aqua regia while potassium dichromate solution was used for etching the bronze samples. Microstructural observations of the polished and etched specimens were carried out using optical microscopy.

Typical tensile fractured surfaces were also examined under a scanning electron microscope (SEM) equipped with a wavelength-dispersive X-ray spectroscopic (WDXS) facility. The specimens were sputtered with gold prior to the SEM examinations.

2.3. Measurement of density, hardness and electrical conductivity

These properties were evaluated using metallographically polished specimens. An average of three observations has been reported in this investigation.

The water-displacement technique was adopted for determining the density of the specimens. A Mettler microbalance was used for the purpose.

Electrical conductivity of the samples was measured using a Technofour type 757 conductivity meter, and hardness measurements were carried out with the help of a Vickers hardness tester at an applied load of 15 kg.

2.4. Tensile tests

Tensile tests were carried out on (22 mm gauge length, 4.0 mm gauge diameter) specimens using a universal testing machine (UTM). Test temperatures adopted were 35, 60, 100, 150 and 200 °C. Strain rates used for the room-temperature tests (35 °C) were 3.80×10^{-4}, 1.52×10^{-3}, 1.52×10^{-2} and 1.52×10^{-1} s^{-1}, while at the remaining temperatures the tests were conducted at the strain rate of 1.52×10^{-3} s^{-1}.

Reported tensile data (UTS and per cent elongation) represent an average of three observations.

TABLE I Chemical composition of the experimental alloys

Serial no.	Specimen	Elements (wt%)					
		Cu	Sn	Pb	Zn	Al	Mg
1.	Zinc-based alloy	2.50	–	–	Bal.	27.50	0.03
2.	Bronze	Bal.	7.20	7.30	2.90	–	–

3. Results

The microstructure of the zinc-based alloy is shown in Fig. 1. It reveals the dendrites of primary α surrounded by the eutectoid α + η in the interdendritic regions (Fig. 1a). Regions marked A and B in Fig. 1b clearly reveal the respective phases. The metastable ε phase can also be seen in Fig. 1b (arrowed).

Fig. 2a and b reveal the dendritic microstructure of the bronze. A magnified view clearly depicts the primary α-dendrites along with the Cu–Sn intermetallic in the interdendritic regions (Fig. 2c). Lead was observed to exist as discrete particles (Fig. 2c). Regions marked A, B and C in Fig. 2c represent the α, the Cu–Sn intermetallic and lead particles, respectively. Occasionally, nucleation of lead at and around the Cu–Sn intermetallic compound was also noticed (Fig. 2c, arrowed).

Table II shows the density, hardness and electrical conductivity of the alloys. It may be noted that the zinc-based alloy attained considerably lower density but higher hardness and electrical conductivity than that of the bronze.

The influence of strain rate on the room-temperature tensile properties of the alloys is shown in Fig. 3. Increasing strength and percentage elongation with strain rate may be noted in the figure, irrespective of the alloy system. Further, the zinc-based alloy attained improved properties as compared with those of the bronze (Fig. 3).

Fig. 4 represents the UTS and percentage elongation of the specimens at different test temperatures. Increasing temperature caused a reduction in the

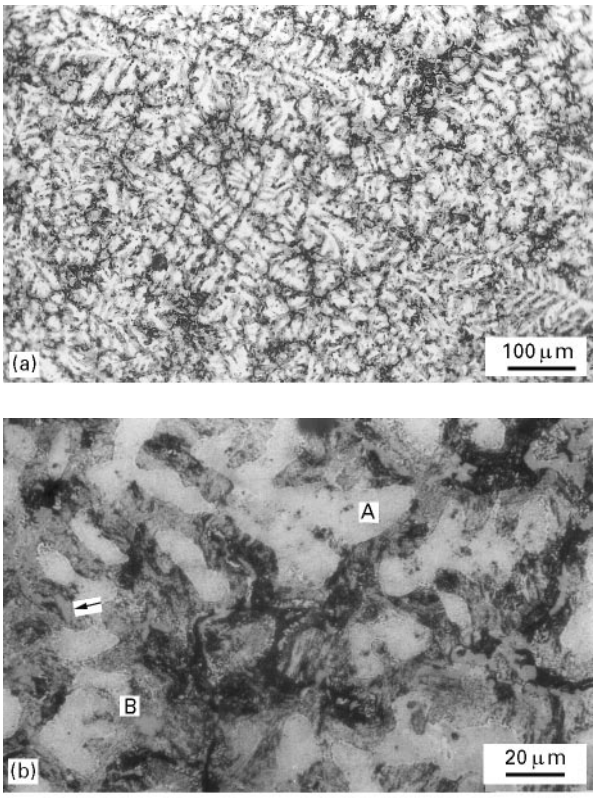

Figure 1 Optical micrographs of the zinc-based alloy revealing (a) the dendritic structure, (b) various microconstituents. A, primary α, B, eutectoid α + η, arrow, ε.

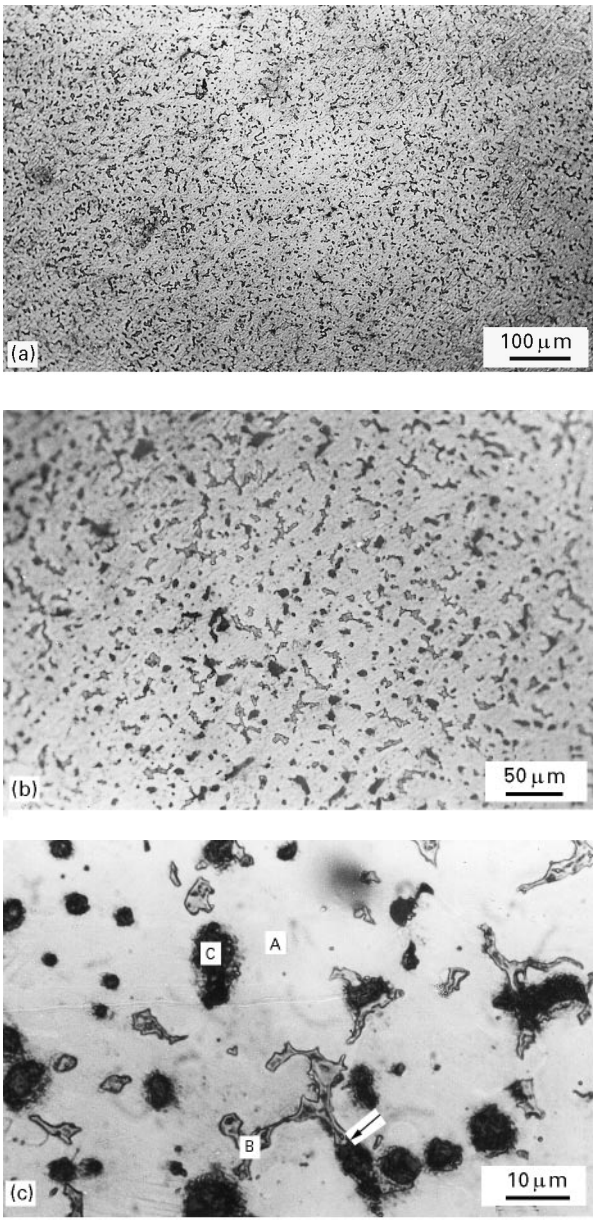

Figure 2 Microstructure of the bronze revealing (a, b) the dendritic structure, and (c) a magnified view depicting the primary α dendrites, A, the Cu–Sn intermetallic compound in the interdendritic regions, B, and lead particles, C, and nucleation of lead around the Cu–Sn intermetallic (arrowed).

TABLE II Properties of the experimental alloys

Serial no.	Specimen	Density ($g\,cm^{-3}$)	Hardness, VHN	Electrical conductivity (% IACS)
1.	Zinc-based alloy	4.97	130	31.0
2.	Bronze	8.85	76	12.0

strength in all the cases, the effect being more marked in the case of the zinc-based alloy. A perusal of the figure also indicates that lower test temperatures led to the attainment of higher strength by the zinc-based alloy as compared to that of the bronze, while test temperatures greater than $\sim 140\,^{\circ}C$ caused a reversal in the trend.

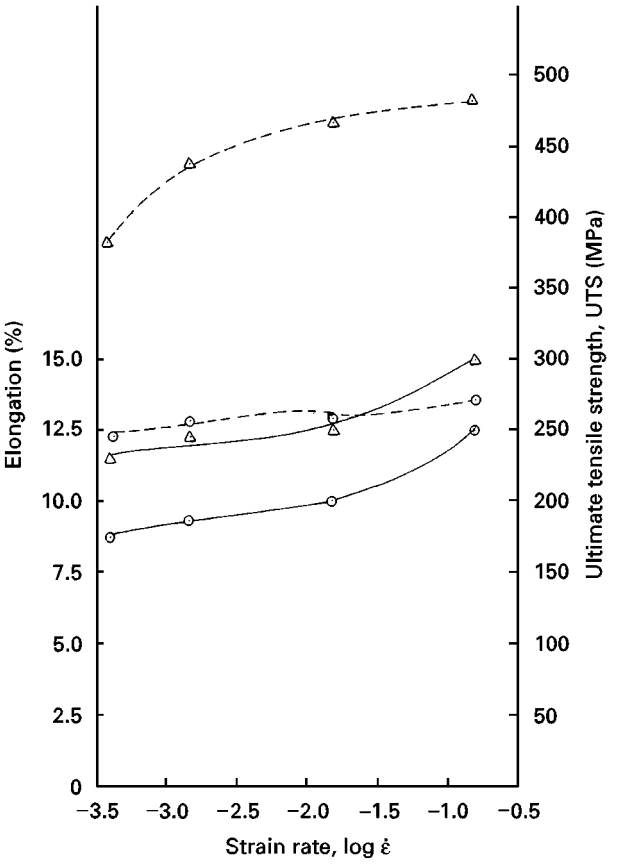

Figure 3 (– – –) Room-temperature ultimate tensile strength (UTS) and (——) percentage elongation as a function of strain rate, for (⊙) bronze and (△) zinc-based alloy.

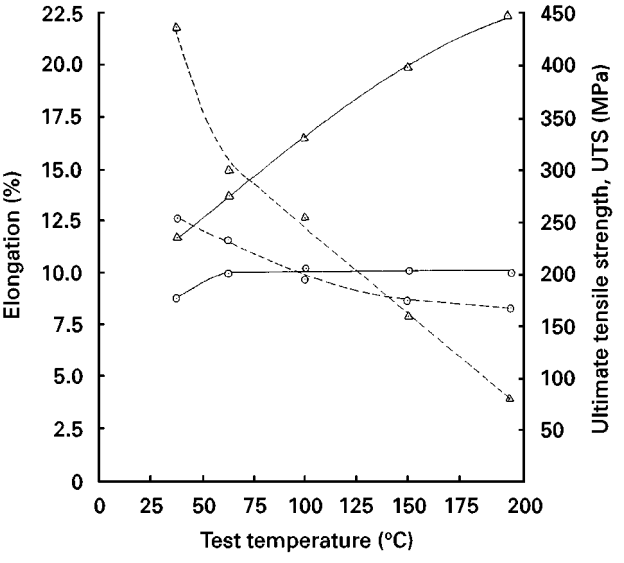

Figure 4 (– – –) Ultimate tensile strength and (——) percentage elongation as a function of test temperature at a strain rate, $\dot{\varepsilon}$, of $1.52 \times 10^{-3}\,s^{-1}$, for (⊙) bronze and (△) zinc-based alloy.

The percentage elongation of the zinc-based alloy was considerably more than that of the bronze over the entire range of test temperatures (Fig. 4). Increasing the test temperature led to higher percentage elongation in both cases, the zinc-based alloy being affected to a larger extent (Fig. 4).

Fractographic features of the zinc-based alloy revealed a mixed mode (brittle and ductile) of fracture in general (Fig. 5). Testing at low temperatures and strain

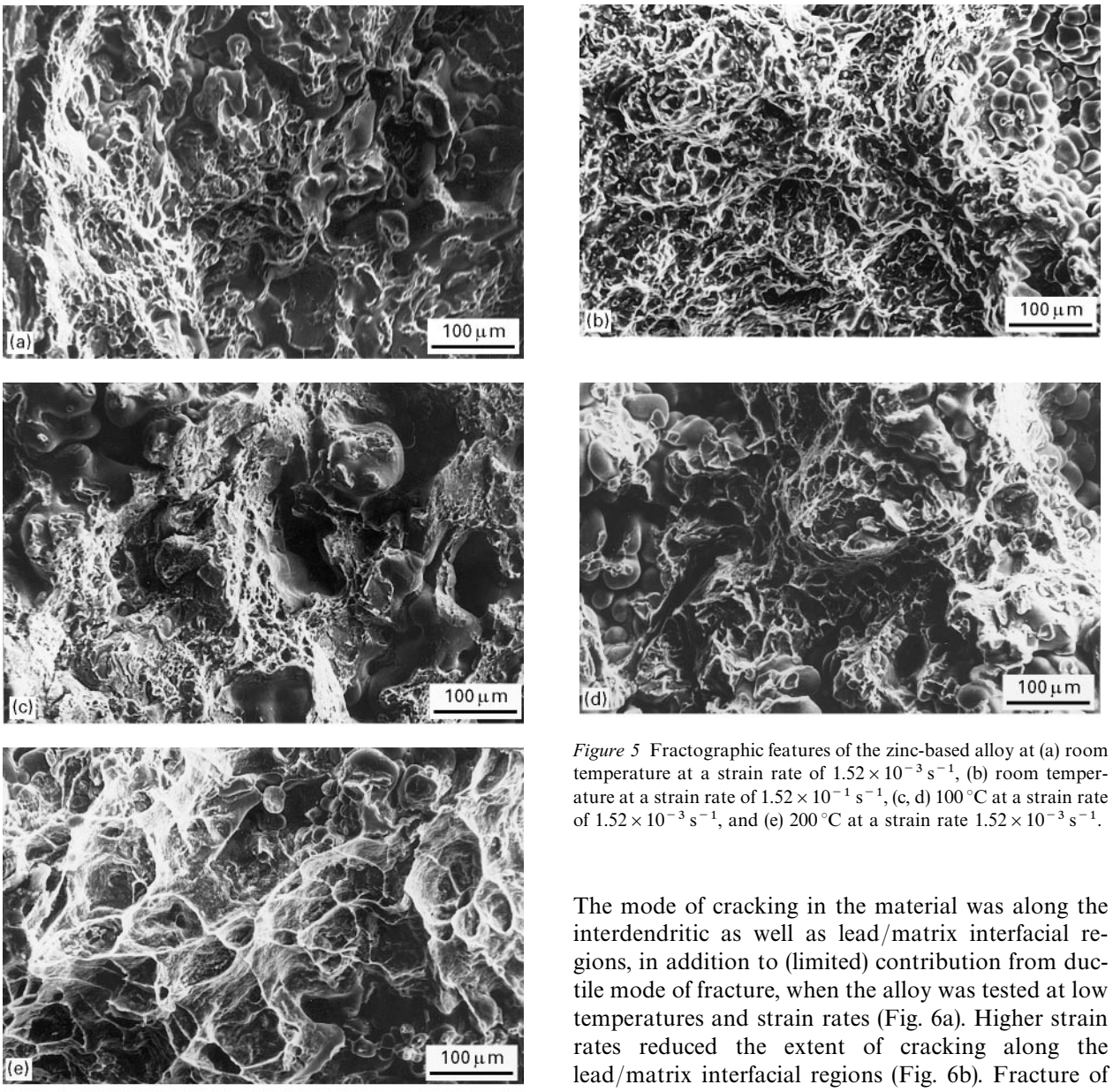

Figure 5 Fractographic features of the zinc-based alloy at (a) room temperature at a strain rate of $1.52 \times 10^{-3}\ s^{-1}$, (b) room temperature at a strain rate of $1.52 \times 10^{-1}\ s^{-1}$, (c, d) 100 °C at a strain rate of $1.52 \times 10^{-3}\ s^{-1}$, and (e) 200 °C at a strain rate $1.52 \times 10^{-3}\ s^{-1}$.

rates led to the formation of plastically deformed regions revealing fine and shallow dimples on the fractured surfaces (Fig. 5a). The presence of regions indicating a brittle mode of failure may also be observed in the figure. Larger strain rates in this case tended to increase the extent of plastic deformation (Fig. 5b). Higher test temperatures indicated a significantly increased contribution of the ductile mode of fracture as evinced by the greater number of dimples on the fractured surfaces (Fig. 5c–e) as compared to that subjected to lower temperature tests at an identical strain rate (Fig. 5a). Moreover, coarsening of the dimples was clearly observed at higher test temperatures (Fig. 5e). The appearance of dendrite-like features over a limited area of the fractured surfaces of the specimens tested at lower temperatures can also be seen in Fig. 5a–d. It may be noted that the proportion of the area comprising the feature decreased with increasing strain rate and temperature (Fig. 5a–d).

Fracture of the bronze occurred by ductile and brittle modes (Fig. 6) as in the zinc-based alloy (Fig. 5). The mode of cracking in the material was along the interdendritic as well as lead/matrix interfacial regions, in addition to (limited) contribution from ductile mode of fracture, when the alloy was tested at low temperatures and strain rates (Fig. 6a). Higher strain rates reduced the extent of cracking along the lead/matrix interfacial regions (Fig. 6b). Fracture of a typical lead particle in this case can be noticed in Fig. 6c (arrowed). That the particle was lead could be confirmed through WDXS analysis (Fig. 6d and e). The extent of the ductile mode of fracture increased somewhat at higher test temperatures (Fig. 6f).

4. Discussion

In zinc-based alloys, aluminium constitutes one of the major elements along with copper and a little magnesium [1, 5, 21]. The alloy studied in this investigation was of hypereutectoid type when considered on the basis of the zinc–aluminium binary equilibrium diagram [22]. The solidification of the alloy begins with the formation of the aluminium-rich solid solution, α (Fig. 1b), depleting the aluminium content of the remaining liquid [10]. This is followed by the eutectoid transformation in the liquid at 275 °C along the interdendritic regions (Fig. 1b). The metastable phase, ε (Fig. 1b), forms due to the presence of more than 1.0% copper in the alloy under the conditions of normal cooling [10, 22–24]. The dark phase in the centre of the interdendritic boundaries in Fig. 1b is the zinc-rich (η) phase [10] whose formation results from

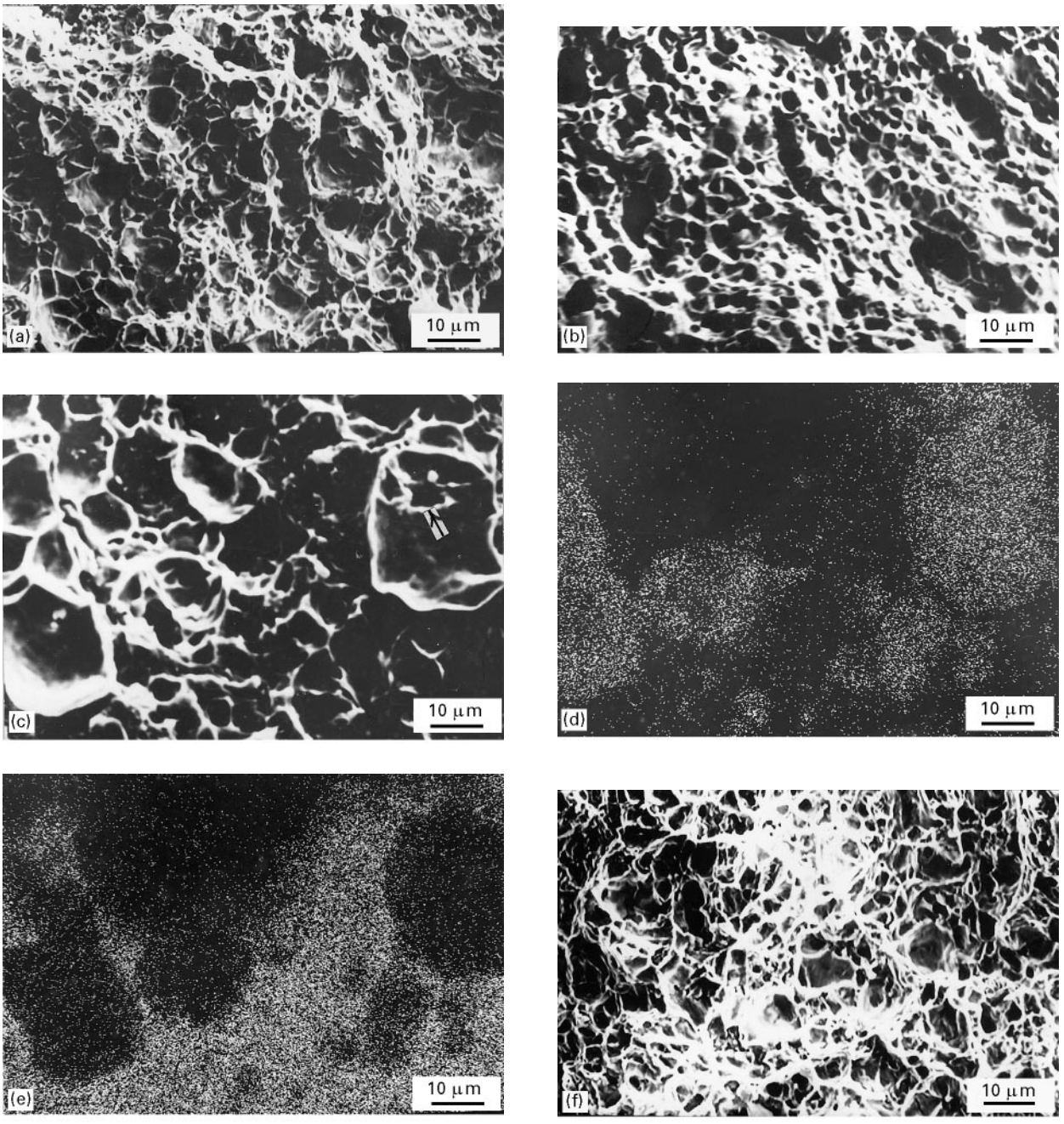

Figure 6 Fractographic features of the bronze tested at (a) room temperature at a strain rate of $1.52 \times 10^{-3}\ s^{-1}$, (b, c) room temperature at a strain rate of $1.52 \times 10^{-2}\ s^{-1}$, (d, e) X-ray dot maps of lead and copper, respectively, corresponding to (c), and (f) 200 °C at a strain rate $1.52 \times 10^{-3}\ s^{-1}$. Cracking of lead is indicated by the arrow.

the wide freezing range of the zinc-based alloy system and local microsegregation of zinc due to the large difference in the density of the element compared with that of aluminium [1].

In leaded-tin bronzes, the first phase to solidify is primary α (solid solution of tin in copper). During solidification, the phase rejects tin, making the remaining liquid rich in the element. This, associated with the wide freezing range of the Cu–Sn system (due to a large difference in the melting point of copper and tin), causes heavy coring [25, 26]. As a result, tin-rich liquid around the primary (α) dendrites occurs. In a Cu–8.0% Sn alloy (which is ideally a single-phase alloy), the concentration of tin in the liquid surrounding the α phase has been observed to be up to ~13.5% [25] which causes the formation of the Cu–Sn intermetallics [25, 26], as shown in Fig. 2b and c. Lead remains in the microstructure as discrete particles (Fig. 2) in view of its very slight solid solubility in copper at room temperature which is negligibly affected in the presence of tin [27]. Nucleation of lead particles on and around the Cu–Sn intermetallic compound (Fig. 2c) could be attributed to the easy centres for the nucleation of the phase offered by the previously forming (Cu–Sn) intermetallic compound. Similarly, the first forming primary α dendrites favoured the nucleation and solidification of lead in the interdendritic regions. Saturation of these sites caused the lead particles to solidify randomly in the matrix (Fig. 2b and c).

The zinc-based alloy attained considerably reduced density than the bronze (Table II) due principally to

the presence of a large quantity of aluminium in the former. The presence of the soft lead particles was responsible for the lower hardness of the leaded-tin bronze over the zinc-based alloy (Table II). The element also caused the bronze to attain lower electrical conductivity than the zinc-based alloy (Table II).

The fracture behaviour of materials during tensile loading depends on two factors, namely their strain-hardening capability and their tendency towards microcracking [28]. Strain hardening is caused by increased dislocation density in the course of deformation [28] and leads to improved tensile properties. In a specified range of strain rates, an increasing strain rate brings about better tensile strength and elongation [22, 28–33]. On the contrary, the cracking tendency of the material has a reverse effect [28]. The presence of microporosity, inclusions, phases having poor compatibility with the matrix, weaker microconstituents and stress-raiser points in the material, make it prone to microcracking. Under a given set of loading conditions, the response of the material depends on the counteracting effects of the mentioned factors, i.e. strain hardening and microcracking tendency.

It may be noted that at low strain rates, the applied (tensile) stress becomes slowly effective towards causing fracture in view of the low crosshead speed. Under the circumstances, a larger fraction of the gauge area shares the stress prior to causing material failure. This also enables the inhomogeneity, weaker spots (e.g. lead in the bronze and the cored zinc-rich phase (η) in the zinc-based alloy, Figs 1 and 2), as well as stress-raiser points (such as interfacial regions) to be more effective in controlling the fracture behaviour of the material [34]. As a result of the enhanced microcracking tendency due to the factors mentioned, the tensile properties of the alloys were less at low strain rates (Fig. 3). However, these factors had insufficient time to show their negative influence when the tests were conducted at higher strain rates and hence the specimens exhibited better properties (Fig. 3).

The lower UTS of the bronze at room temperature than the zinc-based alloy could be attributed to the presence of weak lead particles in the matrix of the former. It may be noted that the weaker lead particles act as void initiators [35, 36] during the process of deformation in view of their poor compatibility with the matrix due to the limited solubility of lead in copper [3, 27]. This enhanced the tendency of microcracks to nucleate and propagate along the lead particle/matrix interfacial regions by way of the dislocations accumulated there during deformation [28]. Interaction of the dislocations with lead particles facilitates nucleation of cracks [28, 35], thereby producing local decohesion along the lead/matrix interfacial regions [28, 36]. Joining of such cracks caused the fracture of material to occur (Fig. 6a). The microcracking of lead particles (Fig. 6c) suggests that although load was transferred to them during deformation, they could not contribute to arresting/delaying failure due to their poor load-bearing capacity. Rather, their microcracking facilitated crack formation (Fig. 6a–c) by way of decohesion in the regions [28, 36]. This, leading to the initiation of brittle failure in the surrounding regions (Fig. 6a–c), was also responsible for the lower percentage elongation of the alloy (Figs 3 and 4). Higher test temperatures made the lead particles, as well the matrix, viscoplastic, so that failure occurred in these regions even without allowing cracks to nucleate at, and propagate along, the lead/matrix interfacial regions. This was perhaps the reason why fracture of lead could not be noticed on the fractured surfaces of the specimens tested at 200 °C (Fig. 6f). At the same time, due to better flowability at the temperature [11], the matrix participated to a larger extent in sharing the tensile load. This caused the percentage elongation of the alloy to increase at higher test temperatures while the UTS reduced (Fig. 4). Owing to the high melting point of the bronze matrix, the strength and percentage elongation of the alloy was not much affected by the test temperature (Fig. 4).

The zinc-based alloy does not contain any weak phase (except a minor quantity of the η phase segregated in the interdendritic boundaries) unlike lead in the case of the bronze. The microstructure of the former contained basically a mixture of two solid solutions, α and η, distributed in a specific manner (Fig. 1). In addition, a minor quantity of ε phase also exists in the microstructure. The solid solutions (α and η) share load without easily allowing microcracks to nucleate at the second-phase particles and/or propagate within the matrix. The presence of the ε phase (as well as the segregated η) does not seem to have any significant (negative) effect in this sense, in view of its low concentration in the microstructure (Fig. 2b) and better compatibility with the matrix. This helped the zinc-based alloy to attain higher strength than the leaded-tin bronze at lower temperatures (Fig. 4). However, at higher temperatures, the lower melting point of the zinc-based alloy, in general, and the interdendritically segregated η, in particular [10], made it less stable and more viscoplastic thus causing its strength to decrease and percentage elongation to improve over that of the bronze (Fig. 4).

The presence of dendrite-like features on the fractured surfaces of the zinc-based alloy tested at low temperatures and strain rates (Fig. 5a–d) has been attributed to the nucleation and propagation of cracks along the regions [34, 37] in view of the generation of shrinkage porosity (preferably along the interdendritic regions) in the alloy system during solidification [37]. However, in the presently studied alloy, practically no porosity but limited segregation of the zinc-rich phase (η) in the interdendritic regions was noted (Fig. 1b). In view of this, the major contribution towards causing fracture of the alloy along the interdendritic regions seems to be from the segregated weak zinc-rich phase in this investigation.

5. Conclusions

1. The zinc-based alloy attained lower density but higher electrical conductivity and hardness than the leaded-tin bronze. A large quantity of aluminium in the former was responsible for its reduced density and higher electrical conductivity. The presence of softer

lead particles in the bronze caused its hardness to be low.

2. Soft and weak lead particles deteriorated the tensile properties of the bronze over that of the zinc-based alloy at low test temperatures. However, a higher melting point of the bronze matrix reduced the influence of temperature on its properties. As a result, the UTS of the bronze was greater than the zinc-based alloy while the percentage elongation followed a reverse trend at higher temperatures.

3. Elevated test temperatures deteriorated the UTS but increased the percentage elongation of the alloys. The properties of the zinc-based alloy were affected much more than those of the bronze under the same circumstances.

4. In the case of the leaded-tin bronze, the mechanisms of material failure at lower temperatures involved the nucleation of microcracks at the lead/matrix interface followed by its propagation along the regions. Fracture of lead was also observed in this temperature range. The above-mentioned phenomena were greatly suppressed at elevated test temperatures due to the viscoplastic characteristics attained by lead and improved flowability of the matrix, ultimately causing relatively more dimples to form on the fractured surface.

References

1. D. APELIAN, M. PALIWAL and D. C. HERRSCHAFT, *J. Metals* **33** (1981) 12.
2. D. KANIKI, *Modern Castings* March (1979) 49.
3. T. CALAYAG and D. FERRES, in "Proceedings of the Earthmoving Industry Conference, 19–21 April 1982, Peoria, IL.
4. W. MIHAICHUK, *Modern Castings* July (1981) 39.
5. K. J. ALTORFER, *Met. Prog.* November (1982) 29.
6. E. GERVAIS, R. J. BARNHURST and C. A. LOONG, *J. Metals* **37** (1985) 43.
7. E. GERVAIS, H. LEVERT and M. BESS, *Trans. AFS* **68** (1980) 183.
8. P. P. LEE, T. SAVASKAN and E. LAUFER, *Wear* **117** (1987) 79.
9. E. J. KUBEL Jr, *Adv. Mater. Proc.* **132** (1987) 51.
10. L. D. BAILEY, S. DIONNE and S. H. LO, in "Fundamental Relationships between Microstructure and Mechanical Properties of Metal Matrix Composites", edited by P. K. Liaw and M. N. Gungor (The Minerals, Metals and Materials Society, 1990) pp. 23–5.
11. P. N. DENT and S. MURPHY, in Proceedings of the International Symposium on Zinc–Aluminium (ZA) Casting Alloys", 25th Annual Conference of Metallurgists, edited by G. P. Lewis, R. J. Barnhurst and C. A. Loong, CIM, (1986), pp. 127–42.
12. C. A. LOONG, *ibid.*, pp. 157–68.
13. E. GERVAIS, M. LEFEBVRE and C. A. LOONG, in "Proceedings of the 13th SDCE International Diecasting Congress and Exposition", paper no G – T 85-055 (1985) pp. 1–8.
14. C. A. LOONG, in "Proceedings of the 14th SDCE International Diecasting Congress and Exposition", Paper no G – T 87-027 (1987) pp. 1–7.
15. N. MYKURA and S. MURPHY, in Proceedings of the International Symposium on Zinc–Aluminium (ZA) Casting Alloys", 25th Annual Conference of Metallurgists, edited by G. P. Lewis, R. J. Barnhurst and C. A. Loong (eds.), CIM, (1986) pp. 45–55.
16. H. LEHUY, *J. Mater. Sci.* **23** (1988) 2943.
17. D. M. RTAPLIN, G. L. DUNLOP and T. G. LANGDON, *Ann. Rev. Mater. Sci.* **9** (1979) 151.
18. F. A. MOHAMMED, M. M. I. AHMED and T. G. LANGDON, *Metall. Trans.* **8A** (1977) 933.
19. K. N. MELTON and J. D. EDINGTON, *Met. Sci. J.* **7** (1973) 172.
20. R. B. NICHOLSON, in "Electron Microscopy and Structure of Materials", edited by G. Thomas (Berkely University, California Press, 1972) p. 689.
21. R. GUERRIERO, J. B. PARCE and I. TANGERINI, in "Proceedings of the International Symposium on Zinc–Aluminium (ZA) Casting Alloys", 25th Annual Conference of Metallurgists, CIM, edited by R. J. Barnhurst and C. A. Loong (1986) pp. 229–248.
22. S. MURPHY, *Z. Metallkde* **71** (1980) 96.
23. G. WALMAG, M. LAMBERIGHTS and D. GUETSOURADIS, in "Proceedings of the International Conference on Zinc–Aluminium (ZA) Casting Alloys", 25th Annual Conference of Metallurgists, CIM, edited by G. P. Lewis, R. J. Barnhurst and C. A. Loong (1986) pp. 5–22.
24. S. MURPHY and T. SAVASKAN, *Wear* **98** (1984) 151.
25. C. R. BROOKS (ed.), "Heat Treatment, Structure and Properties of Non-Ferrous Alloys" (ASM, Metals Park, OH, 1982) pp. 275–82.
26. R. W. HEINE and P. C. ROSENTHEL (eds), "Principles of Metal Casting" (McGraw-Hill, 1955) pp. 308–31.
27. W. A. GLAESER, in "Proceedings of the International Conference on Wear of Materials" edited by K. C. Ludema (ASME, Denver, 1989) pp. 255–60.
28. T. S. SRIVATSAN, S. ANAND and T. S. SUDARSHAN, *Mater. Sci. Technol.* **10** (1994) 640.
29. C. Y. LIN, H. B. McSHANE and R. D. RAWLINGS, *ibid.* **10** (1994) 659.
30. T. HIKOSAKA, T. IMAI, T. G. NIEH and J. WADSWORTH, *Scripta Metall.* **31** (1994) 1181.
31. S. MITRA, *J. Mater. Sci. Lett.* **13** (1994) 1296.
32. G. L. DUNLOP and D. M. R. TAPLIN, *J. Mater. Sci.* **7** (1972) 84.
33. S. SAGAT and D. M. R. TAPLIN, *Acta Metall.* **24** (1976) 307.
34. F. ASHRAFIZADEH, J. M. YOUNG and V. KONDIC, *Mater. Sci. Technol.* **3** (1987) 665.
35. J. P. PATHAK and S. N. TIWARI, *Wear* **155** (1992) 37.
36. B. S. MAZUMDAR, A. H. YEGNESWARAN and P. K. ROHATGI, *Mater. Sci. Eng.* **68** (1984) 85.
37. M. A. SAVAS and S. ALTINTAS, *J. Mater. Sci.* **28** (1993) 1775.

Received 23 February
and accepted 31 July 1996